4548 *Biochemistry* **2009,** *48,* 4548–4556
DOI:10.1021/bi9002887

BIOCHEMISTRY
including biophysical chemistry & molecular biology
Article

Role of Loop−Loop Interactions in Coordinating Motions and Enzymatic Function in Triosephosphate Isomerase[†]

Yan Wang,[‡] Rebecca B. Berlow,[§] and J. Patrick Loria*[,‡,§]

[‡]*Department of Chemistry, Yale University, New Haven, Connecticut 06520, and* [§]*Department of Molecular Biophysics and Biochemistry, Yale University, New Haven, Connecticut 06520*

Received February 19, 2009; Revised Manuscript Received March 31, 2009

ABSTRACT: The enzyme triosephosphate isomerase (TIM) has been used as a model system for understanding the relationship between protein sequence, structure, and biological function. The sequence of the active site loop (loop 6) in TIM is directly correlated with a conserved motif in loop 7. Replacement of loop 7 of chicken TIM with the corresponding loop 7 sequence from an archaeal homologue caused a 10^2-fold loss in enzymatic activity, a decrease in substrate binding affinity, and a decrease in thermal stability. Isotope exchange studies performed by one-dimensional ^{1}H NMR showed that the substrate-derived proton in the enzyme is more susceptible to solvent exchange for DHAP formation in the loop 7 mutant than for WT TIM. TROSY-Hahn Echo and TROSY-selected $R_{1\rho}$ experiments indicate that upon mutation of loop 7, the chemical exchange rate for active site loop motion is nearly doubled and that the coordinated motion of loop 6 is reduced relative to that of the WT. Temperature dependent NMR experiments show differing activation energies for the N- and C-terminal hinges in this mutant enzyme. Together, these data suggest that interactions between loop 6 and loop 7 are necessary to provide the proper chemical context for the enzymatic reaction to occur and that the interactions play a significant role in modulating the chemical dynamics near the active site.

Flexible loops are essential for many critical aspects of protein function including enzyme specificity (*1*, *2*), enzyme catalytic processes (*3*−*5*), and protein−protein interactions (*6*, *7*). Triosephosphate isomerase (TIM[1], EC 5.3.1.1) represents another well documented case of the importance of a flexible loop for proper functioning. TIM catalyzes the rapid and efficient reversible isomerization of an aldehyde, glyceraldehyde 3-phosphate (GAP), and a ketone, dihydroxyacetone phosphate (DHAP), via an enediolate intermediate, which appears not to accumulate on the enzyme to a significant extent (*8*). TIM performs this reaction without the use of metal ions or cofactors. The proper functioning of TIM relies largely on the 11-residue flexible active site loop 6 (*9*) (166-PVWAIGTGKTA-176). In its open conformation, the active site is accessible to solvent, whereas in the Michaelis complex, loop 6 occupies the closed conformation, which sequesters the enzymatic reaction from solvent (Figure 1). Loop 6 moves between these open and closed forms regardless of the occupancy of the active site by substrate (*10*). Solid and solution state NMR as well as fluorescence studies indicate that this motion occurs on a time scale comparable to that of catalytic turnover, suggesting that this conformational change at least partially limits the overall enzymatic reaction rate (*10*−*15*), in agreement with the observation of a viscosity dependence on the k_{cat} value (*16*). The importance of loop 6 flexibility in TIM function has been addressed in great detail through biochemical experiments that demonstrated its essential flexibility in facilitating the enzymatic reaction (*17*) and in defining the interactions within loop 6 and between residues from loop 6 and nearby loop 7 that are crucial in stabilizing the closed, active form (*16*, *18*). The primary sequence of loop 6 is highly conserved, and mutagenesis experiments and biophysical studies have helped define the sequence requirements necessary for optimal coupling of loop 6 motion and enzyme function (*19*−*23*).

Thorough biochemical studies have been carried out to identify crucial interactions in TIM, and comparison of these data with sequences and crystal structures of homologous enzymes revealed a strong relationship between the sequences of loop 6 and loop 7 (*24*). The presence of the N-terminal hinge sequence (166-PVW) of loop 6 appears to always correlate with the 208-YGGS motif in loop 7. Deviations from the PVW sequence, typically 166-PPE (using chicken TIM numbering), result in corresponding changes in loop 7 sequences to 208-CGAG or, most commonly, 208-TGAG (Supporting Information). These deviations from the loop 6/loop 7 PVW/YGGS sequence typically occur in archaeal organisms such as *T. tenax* and *P. woesei*. In other organisms, loop 7 aids in stabilizing the closed conformation of loop 6 by providing hydrogen-bonding interactions between the η oxygen of Tyr208 and the amide nitrogen of Ala176 (*11*, *16*). Additionally, the γ oxygen of Ser211

[†]J.P.L. acknowledges support from NIH (R01-GM070823). R.B.B. thanks the NIH for biophysical training grant support (5T32GM008283).

*Corresponding author. Phone: 203-436-4847. Fax: 203-432-6144. E-mail:patrick.loria@yale.edu.

[1]Abbreviations: TIM, chicken triosephosphate isomerase; TGAG, loop 7 mutant sequence changed from YGGS to TGAG.

Published on Web 4/6/2009

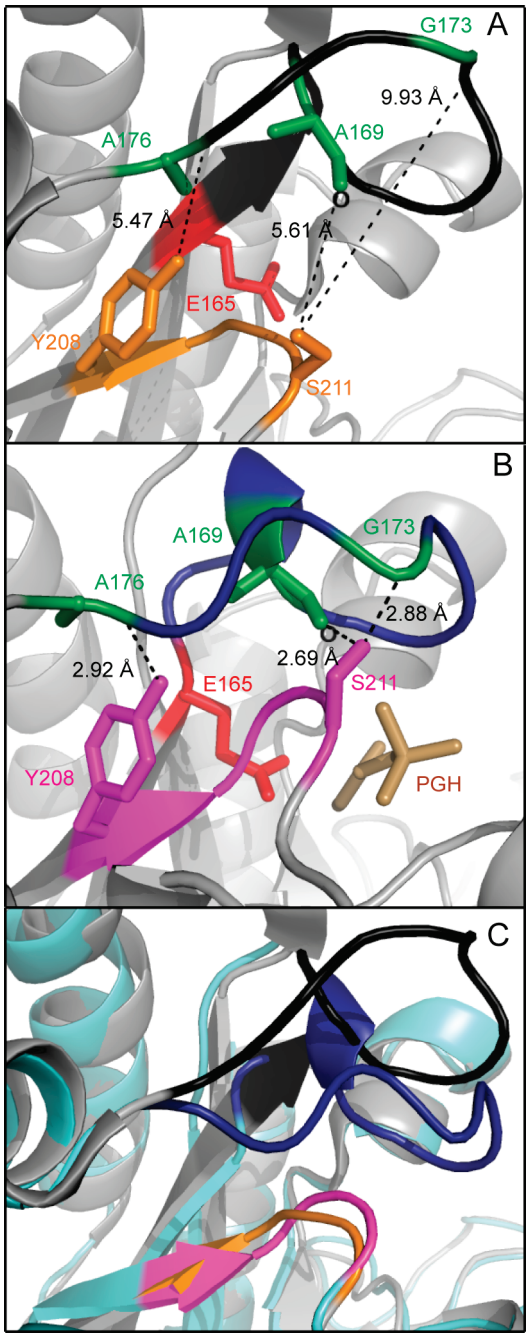

FIGURE 1: Cartoon rendering of loop structures in cTIM. (A) Open conformation of apo cTIM. Loop 6 is colored black, loop 7 in orange, E165 in red, and A169, G173, and A176 in green. Hydrogen bonds between the two loops are shown as black dashed lines, with corresponding distances indicated in black. (B) Closed conformation of bound cTIM using the same color scheme as in A except for loop 6, which is colored blue, loop 7, which is magenta, and phosphoglycolohydroxamate (PGH) (*27*), which is brown. (C) Overlay of open (gray) and closed (cyan) conformations of cTIM. Loops are colored in the same scheme used in A and B.

participates in hydrogen bonding with the backbone carbonyl oxygen of Ala169 and the amide nitrogen of Gly173. Like loop 6, the YGGS motif of loop 7 occupies two conformations (Figure 1). When loop 6 moves from the open to the closed conformation, the peptide bond between Gly209 and Gly210 in loop 7 rotates by 90°, and the peptide bond of Gly210 and Ser211 flips such that the ϕ/ψ angles of Ser211 change from −80°/120° to 65°/30°. The former motion enables the catalytic base Glu165 to move ~2 Å into its catalytically competent conformation, while the latter motion allows the backbone amide nitrogen of Ser211 to interact with the substrate's phosphate group (*24*−*26*). Interestingly, there are no observed hydrogen bonding or electrostatic interactions between loop 7 and the N-terminal hinge (PVW) region of loop 6 (*24*).

In this work, we addressed the interactions between loop 6 and loop 7 by replacing the 208-YGGS portion of loop 7 with its archaeal counterpart 208-TGAG. Using biochemical and biophysical experiments, we found that loop 7 acts to coordinate the concerted motion of loop 6, helps maintain optimal catalysis, and plays a role in TIM thermal stability.

MATERIALS AND METHODS

Materials. All reagents were purchased from Sigma-Aldrich (St. Louis, MO) unless otherwise indicated. Stable isotopes including $^{15}NH_4Cl$, U-$^{13}C_6$-Glucose, and D_2O for protein expression and labeling were purchased from Cambridge Isotope Laboratories (Andover, MA). Oligonucleotides for mutant enzyme construction were synthesized at the W. M. Keck Facility (Yale University).

Protein Expression. All protein expression was carried out in *E. coli* strain BL21(DE3). Cell cultures were grown in the presence of 100 μg/mL carbenicillin at 37 °C with shaking at 225 rpm. For NMR sample preparation, a single colony was selected to inoculate a starter culture in LB rich medium and grown to midlog phase. One milliliter of this culture was transferred to a small culture of M9 minimal medium [0.4%(w/v) glucose] in 50% D_2O and was grown overnight. This entire culture was then transferred to 1 L of M9 in 99% D_2O and grown to an OD_{600} of 0.6−0.8, at which point 0.8 mM isopropyl 1-thio-D-galactoside (IPTG) was added to induce protein expression at 30 °C. Uniform isotopic labeling of ^{15}N and ^{13}C was achieved using $^{15}NH_4Cl$ and U-$^{13}C_6$-Glucose as the nitrogen and carbon sources, respectively. Cells were harvested by centrifugation after 16 to 18 h of induction. Unlabeled protein for biochemical studies was expressed under the same conditions using LB as the growth medium.

Protein Purification. The *E. coli* cell pellet was lysed by two cycles of sonication in 10 mM Tris-HCl buffer at pH 7.5 in the presence of 1 mM PMSF as a protease inhibitor. Clarified crude cell lysate was loaded onto a DEAE-FF ion-exchange column (Amersham Biosciences/GE Healthcare, Piscataway, NJ) and eluted with the same buffer and a linear concentration gradient of KCl from 0 to 60 mM over a total volume of 400 mL at a flow rate of 2 mL/min. Fractions were analyzed by SDS−PAGE, and those containing cTIM were pooled and desalted using an Amicon Centriprep Concentrator with a MWCO of 10,000 kDa (Amicon, Danvers, MA). Pooled fractions were loaded onto the DEAE-FF column a second time to remove minor contaminants and remaining traces of DNA. Eluted fractions containing cTIM were determined to be more than 95% pure by SDS−PAGE and were pooled and dialyzed against appropriate buffers as described in later sections. The protein was then concentrated to a final volume of ~550 μL and stored at 4 °C. Protein concentration was determined by UV absorbance at 280 nm with the extinction coefficient of 44,400 M^{-1} cm^{-1} for dimeric wild-type (WT) cTIM and 42,400 M^{-1} cm^{-1} for dimeric loop 7 mutant (TGAG). The dimeric extinction coefficient for the loop 7 mutant was obtained by scaling the WT value with the ratio of monomeric extinction coefficients for two constructs calculated from their primary sequences. The final protein yield was about 30 mg from 1 L of growth.

Mutagenesis. The plasmid containing the sequence of WT cTIM cloned into bacterial expression vector pET-15b was a generous gift from Professor Nicole Sampson (State University of New York, Stony Brook, NY). The 208-YGGS to 208-TGAG mutant was constructed using site-directed mutagenesis via three sequential steps due to the large number of mismatched base pairs. In the first step, mutation to Y208T was performed with primers 5′-G TCA ACT AGG ATC ATC ACT GGA GGT TCA GTC ACT GG-3′(sense) and 5′-CC AGT GAC TGA ACC TCC AGT GAT GAT CCT AGT TGA C-3′(antisense). In the second step, mutation to G210A was performed using the DNA template from the first step and primers 5′-T AGG ATC ATC ACT GGA GCT TCA GTC ACT GGT GGC-3′ (sense) and 5′-GCC ACC AGT GAC TGA AGC TCC AGT GAT GAT CCT A-3′ (antisense). The final mutation to S211G was performed using the DNA template from the second step and primers 5′-G ATC ATC ACT GGA GCT GGA GTC ACT GGT GGC AAC-3′ (sense) and 5′-GTT GCC ACC AGT GAC TCC AGC TCC AGT GAT GAT C-3′ (antisense). The proper sequence of both mutant plasmid strands was confirmed by DNA sequencing (W. M. Keck Facility at Yale University).

CD Spectroscopy. The circular dichroism experiments to measure the temperature denaturation of TIM were carried out on an Aviv CD spectrometer using a 1.0-mm path length cuvette. TIM samples were dialyzed against NMR buffer containing 10 mM MES at pH 6.6, 10 mM NaCl, 0.02% (w/v) NaN_3, and 7.5% D_2O and diluted to 4 μM with the same buffer. The CD signal at 214 nm was monitored as the temperature was increased from 278 K (5 °C) to 368 K (95 °C) at a rate of 1 °C/min. Nonprotein signals were subtracted using an identically buffered sample without TIM. The mean residue molar ellipticity [θ] was calculated using eq 1

$$[\theta] = \frac{\theta}{N \times M \times l \times 10} \quad (1)$$

where θ is ellipticity measured in millidegrees, N is the number of residues, M is molar concentration, and l is the path length in centimeters.

Enzyme Kinetics. The enzyme kinetic assay was performed at 298 K using GAP as the substrate. TIM samples were dialyzed against 100 mM triethanolamine buffer containing 10 mM EDTA at pH 7.6 (*28*). Enzymes were diluted to ensure the linear dependence of the observed initial rate on the concentrations of enzyme. GAP concentration in the commercial stock was determined enzymatically. The reaction was monitored in the same buffer with a final reaction volume of 1 mL. Samples were prepared by mixing 0.1 mM NADH, 0.02 mg/mL glycerol 3-phosphate dehydrogenase, and 0.8 nM WT cTIM, or 60 nM TGAG TIM. The mixture was equilibrated at 25 °C for 5 min, and the reaction was initiated by adding GAP at a series of concentrations. The initial rate was measured according to the decay of the absorbance at 340 nm at each substrate concentration. The k_{cat} and K_m values for isomerization of GAP were extracted from nonlinear least-squares fitting of the plots of initial rate versus substrate concentration to the Michaelis−Menten equation.

Isotope Exchange Experiments. The TIM-catalyzed conversion of GAP to *d*-GAP, DHAP, and *d*-DHAP was monitored by ^{1}H NMR spectroscopy as described previously (*29*). Briefly, aliquots of the stock solution of GAP were exchanged into D_2O by three cycles of drying under dry nitrogen gas and dissolving in D_2O. Exchanged GAP samples were stored at −20 °C for future use. The pH of GAP in D_2O was adjusted prior to use by the addition of KOD. Samples for NMR analysis contained 15 mM GAP, 20 mM MES, and 10 mM NaCl in 100% D_2O (pD = 6.0). DSS was added as an internal standard to a final concentration of 1 mM. For wild-type enzyme, the final concentration of TIM in the sample was 0.76 nM; for the TGAG mutant, the final enzyme concentration was 15 nM.

^{1}H NMR spectra were collected at 298 K on a Varian Unity Inova 500 MHz spectrometer. Samples were shimmed manually to obtain linewidths ≤0.8 Hz. Each spectrum was recorded with a sweep width of 5500 Hz, 64 transients, and a recycle delay of 80 s. All spectra from the same time course experiment were processed and analyzed identically using the software MestReNova (CambridgeSoft). The time points for each series were taken to be the midpoint of total acquisition time for each spectrum. The time dependence of the concentrations of reactants and products were determined by first normalizing the integrated areas to an internal standard of DSS and by correcting for differential hydration and the number of protons contributing to the signal. The fractional yield of *d*-GAP, *d*-DHAP, and DHAP at each time point was determined relative to its value at $t = 0$ (prior to addition of TIM).

NMR Experiments. All NMR samples were prepared in buffer containing 10 mM MES at pH 6.6, 10 mM NaCl, 0.02% (w/v) NaN_3, and 7.5% D_2O. Samples for NMR spin relaxation experiments were uniformly (^{2}H, ^{15}N) labeled with ∼95% isotope incorporation. Protein concentrations were measured to be 0.8 mM for WT and 1.0 mM for TGAG cTIM. The TGAG sample for assignment experiments was uniformly (^{2}H, ^{13}C, and ^{15}N) labeled, with a final enzyme concentration of 1.0 mM. Resonance assignments for WT cTIM were obtained from BMRB entry 15064 (*19*). Many resonances in the loop 7 mutant (TGAG) could be assigned by comparison of ^{15}N HSQC spectra with those of WT cTIM. These assignments were confirmed, and ambiguities were resolved using data from a TROSY-based HN(CA)CB experiment (*30*−*32*). For the TGAG enzyme to simulate the substrate bound conformation, the substrate analogue glycerol-3-phosphate (G3P) was titrated to the loop 7 mutant until saturation. The NMR assignments of the bound form were obtained as described above.

NMR experiments were performed at a static magnetic field strength of 14.1 T on a Varian Inova spectrometer equipped with a room temperature triple-resonance probe and triple-axis gradients. All NMR experiments were conducted at temperatures that were calibrated using 100% methanol as a standard. NMR data was processed using NMRPipe (*33*) and analyzed using Sparky (*34*) in conjunction with in-house written programs for dispersion fitting. WT and TGAG NMR experiments were collected with identical parameters using spectral widths of 2400 × 8000 Hz and 256 × 2048 points in the t_1 and t_2 dimensions. Peak heights were quantitated in Sparky using the average of nine points from a 3 × 3 grid centered on the peak maximum (*35*). Relaxation rates were determined from peak intensities and in-house written programs. Uncertainties in rates were determined from duplicate measurements and the Jackknife procedure (*36*). The results reported here are based only on amino acid residues that are not overlapped in the 2D spectra and that have sufficient signal-to-noise such that reliable quantitation of peak intensities is possible.

Off-resonance TROSY-selected $R_{1\rho}$ experiments were performed using the pulse sequence developed by Palmer and

co-workers (*37*). The field strength of the spin-locking radio frequency pulse was calibrated prior to each experiment by using off-resonance continuous wave decoupling as previously described (*38*, *39*). The measurements for WT were as described previously by Berlow et al. (*11*). For TGAG, the relaxation delays for measuring $R_{1\rho}$ were 2 (×2), 10, 22 (×2), 38, 54, and 80 (×2) ms at each of nine effective field strengths (ω_e). The relaxation delay series was conducted with the spin-lock pulse between 5 and 50 ppm upfield of the ^{15}N carrier, utilizing tilt angles ranging from 30° to 65°. The spin-locking relaxation period was flanked by tan/tan *h* adiabatic pulses (*40*, *41*) that were used to align magnetization along the respective fields (*42*) and return it to the *z*-axis after the relaxation delay. These adiabatic pulses had a duration of 6 ms and were initiated 15 kHz from the spin-lock carrier frequency. To estimate the exchange contribution, R_{ex} ($= p_A p_B \Delta\omega^2/k_{ex}$) to the narrow ^{15}N-β resonance, the TROSY (*31*) based Hahn-Echo experiment was performed as described (*43*) with a relaxation delay of 21.6 ms ($2/J_{NH}$).

The TROSY-selected $R_{1\rho}$ experiment selectively monitors the decay of the narrow (β) component of the TROSY multiplet (*37*). In the presence of an off-resonance RF field, spin-locked ^{15}N magnetization decays as follows:

$$R_{1\rho}^{\beta} = R_1^{\beta}\cos^2\theta^{\beta} + R_2^{\beta}\sin^2\theta^{\beta} \quad (2)$$

in which the longitudinal and transverse relaxation rates in eq 2 are given by

$$R_1^{\beta} = R_1 - \eta_z + \mu_{1H} \quad (3)$$

and

$$R_1^{\beta} = R_2^0 - \eta_{xy} + \mu_{1H} + R_{ex} \quad (4)$$

In eqs 3 and 4, the transverse and longitudinal relaxation interference rates are η_{xy} and η_z, respectively. For large perdeuterated proteins, η_{xy} and R_2^0 largely cancel, and μ_{1H} is additionally minimized by deuteration. The term of interest in these studies is the exchange contribution due to intramolecular motion termed R_{ex} and is given by

$$R_{ex} = \frac{p_A p_B \Delta\omega^2 k_{ex}}{k_{ex}^2 + \omega_e^2}\sin^2\theta^{\beta} \quad (5)$$

In eq 5, $p_{A/B}$ refers to the equilibrium populations of site A/B due to conformational motion. The rate constant for this motion is given by k_{ex} with $\Delta\omega$ being the chemical shift difference for the ^{15}N nucleus in conformations A and B. θ is the tilt angle of the effective field and is equal to $\arctan(\omega_1/\Omega^{\beta})$, where the amplitude of the spin-locking field is ω_1, and Ω^{β} is the offset from the spin-locking field of the β component of the NH doublet. The effective field is given by $\omega_e = (\omega_1^2 + (\Omega^{\beta})^2)^{1/2}$. Measuring $R_{1\rho}^{\beta}$ at multiple ω_e values, termed dispersion analysis, combined with independent measurement of R_1^{β} (*37*) allows the determination of R_2^{β} at each effective field. In the fast exchange limit ($k_{ex} > \Delta\omega$), fitting eq 6 to these data allows determination of k_{ex}, ϕ_{ex}, and $R_2^{0,\beta}$

$$R_2^{\beta} = \frac{\phi_{ex} k_{ex}}{k_{ex}^2 + \omega_e^2} + R_2^{0,\beta} \quad (6)$$

where $\phi_{ex} = p_A p_B \Delta\omega^2$.

As described before, R_{ex} determined from the Hahn-Echo experiment is as follows (*44*–*46*):

$$R_{ex}^{HE} = p_A p_B \Delta\omega^2/k_{ex} \quad (7)$$

RESULTS

Characterization of Loop 7 Mutant TIM. Wild-type (WT) and the loop 7 mutant (TGAG) TIM enzymes were expressed and purified to >95% homogeneity as judged by SDS−PAGE analysis. The correct mutations were confirmed by gene sequencing and subsequently by solution NMR. The thermal stability of each enzyme was assessed by monitoring the change in the circular dichroic (CD) signal at 214 nm as a function of temperature (Figure 2). The thermal melting profiles are irreversible over the temperature range studied. The midpoint of the CD temperature profile was 333 K for WT and 322 K for the TGAG mutant.

The catalytic activity of WT and TGAG mutant enzymes for the conversion of GAP to DHAP was measured at 298 K. For WT TIM, $k_{cat} = 2000 \pm 60\ s^{-1}$, $K_m = 0.46 \pm 0.06$ mM, and $k_{cat}/K_m = 4300 \pm 600\ mM^{-1}\ s^{-1}$. In the TGAG mutant, these values were $k_{cat} = 35 \pm 1\ s^{-1}$, $K_m = 1.96 \pm 0.11$ mM, and $k_{cat}/K_m = 18 \pm 1\ mM^{-1}\ s^{-1}$. The mutation of loop 7 residues results in over 2 orders of magnitude decrease in k_{cat}/K_m largely due to the reduction in k_{cat}.

Isotope Exchange Studies. The incorporation of solvent deuterium into the enzyme derived reaction products was determined by one-dimensional ^1H NMR spectroscopy as described by Richard and co-workers (*29*, *47*)) (Figure 3). When TIM reacts with protonated GAP in 100% D_2O, the enzymatic reaction can yield any of three potential products (Scheme 1). The enzyme reaction with GAP as a substrate starts when the catalytic base E165 abstracts the C2 proton from GAP to form the enediol(ate) intermediate. If this proton remains with E165 rather than exchanging with solvent D_2O then C1 of the enediol will be protonated to form DHAP. If, however, E165 exchanges its substrate-derived proton with a solvent-derived deuteron after this initial enolization, then C1 of DHAP will contain deuterium (*d*-DHAP). Alternatively, deuterated E165 could simply deuterate the enediol intermediate to reform the substrate, but now C2 will be deuterated by the solvent derived deuteron (*d*-GAP).

All three of these enzyme reaction products as well as the initial GAP are resolvable by ^1H one-dimensional NMR (Figure 3). The C1 proton of GAP is a doublet at 5.001 and 4.989 ppm, split by $^3J_{HH}$ with the C2 proton. *d*-GAP is the broad singlet at 4.995 ppm. The C1 proton of DHAP and *d*-DHAP hydrates resonate

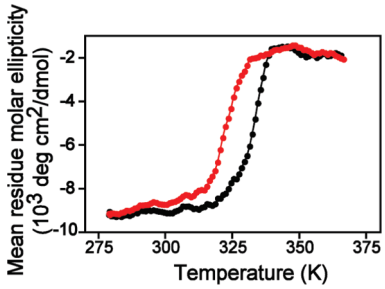

FIGURE 2: Thermal denaturation of cTIM. CD melting curves of WT (black) and TGAG (red) cTIM. θ is monitored at 214 nm at dimeric protein concentrations of 4 μM. The results shown are the average of three repeat measurements for each enzyme.

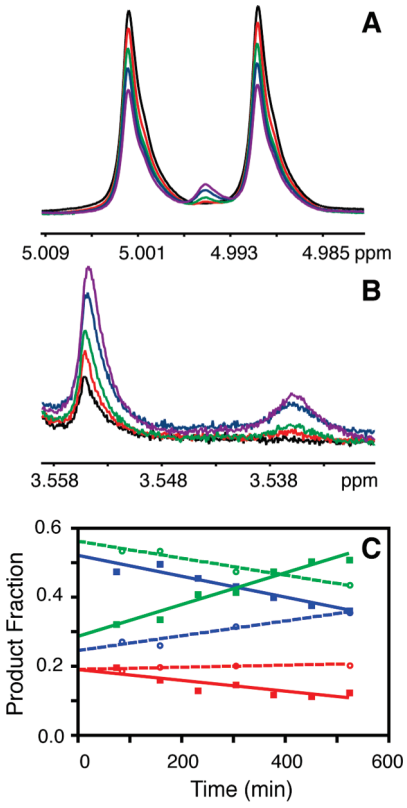

FIGURE 3: Results of isotope exchange studies. Panels A and B: ^{1}H NMR spectra from the isomerization reaction catalyzed by TGAG mutant TIM. Representative regions of the spectra for GAP hydrate (A) and (B) the DHAP hydrate are shown for the following times after the addition of enzyme: 0 min (black), 82 min (red), 156 min (green), 302 min (blue), 522 min (purple). Panel C: product distributions of *d*-GAP (red), *d*-DHAP (green), and DHAP (blue) as a function of time for wild-type TIM (closed squares, solid lines) and TGAG (open circles, dashed lines).

at 3.556 and 3.536 ppm, respectively. The time-dependent change in concentrations of *d*-GAP, GAP, DHAP, and *d*-DHAP are shown in Figure 3 for WT and the TGAG mutant. Analysis of the product fractions as a function of reaction time yields linear plots as observed previously (*20*, *33*). For WT, the fractional yields of products are 0.19 ± 0.01 (*d*-GAP), 0.52 ± 0.01 (DHAP), and 0.29 ± 0.02 (*d*-DHAP). These values obtained for WT chicken TIM are identical to those reported previously for WT chicken and rabbit TIM by Richard and co-workers (*29*). For the TGAG mutant, the fractional yields of products are 0.21 ± 0.02 (*d*-GAP), 0.28 ± 0.03 (DHAP), and 0.50 ± 0.01 (*d*-DHAP). The TGAG loop 7 mutant produces nearly twice as much *d*-DHAP than the WT enzyme, at the expense of protonated DHAP.

NMR Experiments. The NMR resonance assignments of WT TIM were previously determined by triple-resonance TROSY based experiments (*19*). The assignments for TGAG TIM were achieved by comparison with WT enzyme and in combination with a TROSY HN(CA)CB three-dimensional spectrum. In total, 226 nonproline residues were assigned in WT and 207 nonproline residues have been assigned in the TGAG enzyme. A comparison of $^{1}H-^{15}N$ chemical shifts between the two enzymes is shown in Figure 4. The average (per residue) root-mean-square chemical shift deviation between WT and TGAG is $C^{\beta} = 1.2$, $^{N}H = 0.1$, and $^{H}N = 1.0$ ppm. For the WT enzyme, assignments for loop 6 residues were complete and encompass V167−T177, whereas in TGAG all but residue I170 were assigned. In loop 7, only G209 was assigned in WT. There are no unassigned WT peaks in the $^{1}H-^{15}N$ TROSY spectrum, and therefore, it is likely that the missing loop 7 residues are absent due to exchange broadening or overlap with other residues. In the TGAG mutant enzyme, only G209 and A210 in loop 7 were assigned.

In the NMR results below, the main focus is on the N- and C-terminal loop 6 hinge residues V167 and T177. These residues are well resolved in the $^{1}H-^{15}N$ two-dimensional experiments and show significant, nonzero exchange contributions to their transverse relaxation rates. Residues in the center of loop 6 do not show characteristic conformational exchange in the NMR experiments, most likely due to $\Delta\omega \approx 0$ for these flexible residues (*11*, *13*, *43*). Conveniently, because V167 and T177 are at opposite ends of loop 6 their relaxation behavior reports on the relationship and correlation of the motions of these important hinge residues.

The results of the TROSY Hahn-Echo experiment (*43*) (Figure 5A) show that the majority of residues in WT and TGAG mutant TIM do not experience resonance linebroadening due to conformational exchange phenomena (*11*). However, amide positions in loop 6 have elevated R_{ex} values that are indicative of μs−ms motions that modulate the isotropic chemical shift at these positions. For WT, these R_{ex} values are 38.2 ± 2.3 s^{-1} and 11.7 ± 0.7 s^{-1} for V167 an T177, respectively at 298 K, whereas the same residues in the TGAG mutant have R_{ex} values = 37.6 ± 3.3 s^{-1} and 3.7 ± 0.9 s^{-1}. The temperature dependence of R_{ex} allows estimation of an apparent activation barrier for loop closure (*13*). On the basis of these experiments (Figure 5B), the apparent activation barrier for loop closure in WT is 57.6 ± 7.7 kJ/mol and 66.0 ± 4.1 kJ/mol for V167 and T177. In contrast, these values in the loop 7 mutant are 5.9 ± 1.6 kJ/mol and 26.3 ± 10.9 kJ/mol for V167 and T177, respectively. Thus, the barrier for loop 6 closure decreases significantly upon mutation of loop 7. In the presence of saturating amounts of the substrate analogue, glycerol-3-phosphate (G3P) temperature dependent Hahn-Echo experiments for TGAG TIM (not shown) also show different apparent activation energies for the V167 and T177. The barrier to loop 6 opening in the G3P bound form is 69.4 ± 2.9 and 43.9 ± 3.5 kJ/mol. In the WT enzyme with bound ligand, R_{ex} is small and exhibits a slight negative Arrhenius slope. For example, at 293 K R_{ex} for V167 and T177 in G3P bound WT is 1.9 ± 0.8 and 2.3 ± 0.6 s^{-1}, respectively. These small values are likely due to a highly skewed closed population and/or a small value for k_{ex}, with the slight negative slope attributable to the temperature dependence of the equilibrium populations.

Further quantitation of loop 6 conformational motion was obtained from TROSY-selected $R_{1\rho}$ experiments (*37*) as shown in Figure 6. Dispersion of the R_2^{β} values with effective field is indicative of conformational exchange motions. Fitting eq 6 to the WT data yielded a k_{ex} value of 9000 ± 1500 s^{-1} for both V167 and T177 (*11*). The exchange rate constant for the same residues in the loop 7 mutant is increased to 18,000 ± 2000 s^{-1}. For both WT and the loop 7 mutant, fitting of V167 and T177 individually gave very similar k_{ex} values; therefore, both residues were analyzed assuming a single, identical k_{ex} value.

DISCUSSION

Loop regions in proteins are essential for many biological functions, and in triosephosphate isomerase, the active site loop 6

Scheme 1: Reaction of Protonated GAP with TIM in 100% D_2O[a]

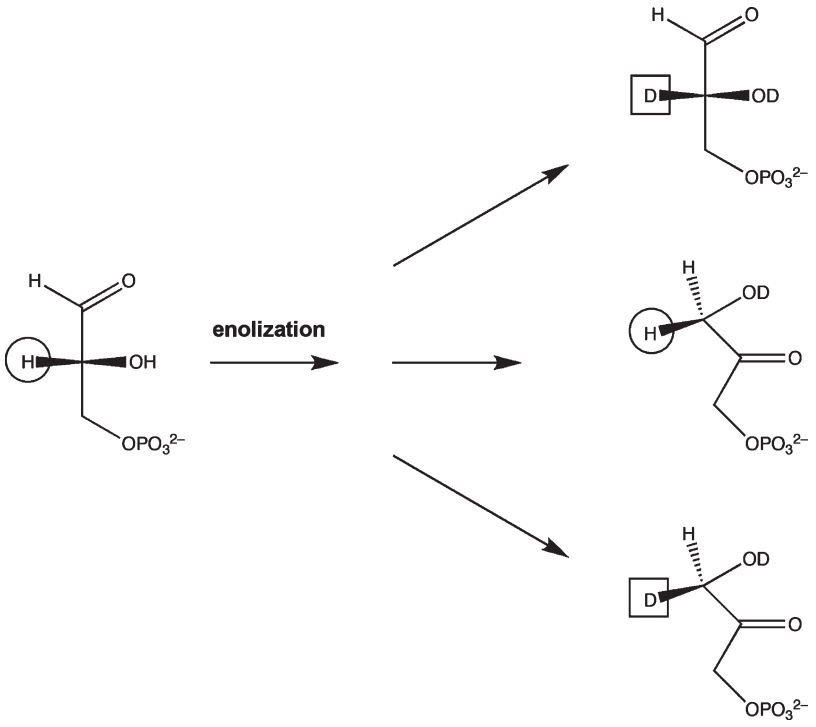

[a] Upon enolization, the C2 proton removed by E165 can be directly placed at C1 to form protonated DHAP, exchanged with solvent to form C1 deuterated DHAP (*d*-DHAP), or exchange with solvent and become C2 deuterated to form deuterated GAP (*d*-GAP). Substrate derived protons are shown in circles, whereas solvent derived deuterons are depicted in squares.

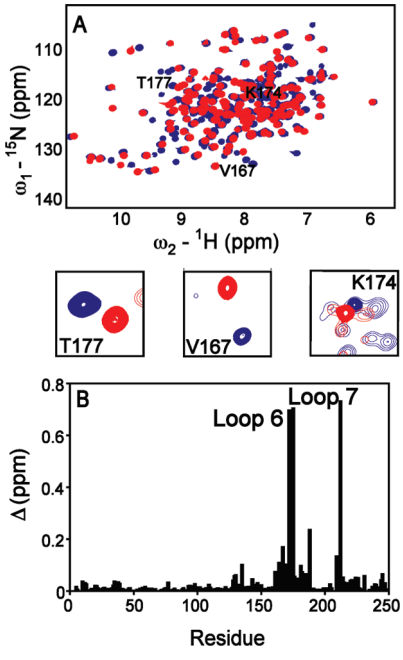

FIGURE 4: Chemical shift changes upon mutation of loop 7. (A) Superimposed $^1H-^{15}N$ TROSY HSQC spectra of WT (blue) and TGAG (red) cTIM at 298 K and 14.1 T, with panels for close-up views of selected loop 6 residues. (B) Composite chemical shift changes between WT and TGAG cTIM as a function of amino acid sequence. Composite chemical shift changes were calculated using the equation $((\Delta\delta^2_{HN} + \Delta\delta^2_N/25)/2)^{1/2}$.

has been demonstrated to be indispensable for optimal catalytic activity (*17*). Genome analysis has revealed that amino acid residues in nearby loop 7 vary specifically with changes in the N-terminal hinge region of loop 6 (*24*) (Supporting Information). To investigate the underlying functional interactions, which must drive this coevolution, the loop 7 sequence TGAG that is usually found with the N-terminal loop 6 sequence PPE was inserted into WT chicken TIM. Thus, this version of loop 7 is out of context in that it finds itself in this mutant TIM enzyme without its normal loop 6 partner.

The effects of changing residues 208-YGGS-211 to 208-TGAG-211 are immediately apparent. Catalytic efficiency is decreased 240-fold compared to that of WT cTIM, and the TGAG mutant enzyme melts 11° lower than the WT enzyme. However, the observation of minor chemical shift changes for only loops 6 and 7 (Figure 4) suggests that the mutation of loop 7 results in relatively small structural perturbations, which are localized to the site of the mutation.

In addition to the deleterious effects of alterations in loop 7 on enzyme function, this mutation has a significant impact on the motion of loop 6 (Figure 5). In WT TIM, the N- (V167) and C- (T177) terminal regions of loop 6 have the same apparent activation barrier for loop closure. This observation is in agreement with previous studies indicating that the hinge residues of loop 6 move in a concerted fashion (*13*, *43*). However, in the loop 7 mutant, the hinge residues of loop 6 both have different activation barriers than observed for the WT enzyme. The activation barriers for the N- and C-terminal hinge residues significantly differ from each other as well, with a much more pronounced reduction in the activation barrier for V167 than T177. Additionally, at 298 K, the mutation to TGAG has no effect on the R_{ex} value for V167 but a substantial effect on that of T177. Collectively, these data suggest that one of the major roles of loop 7 is to aid or coordinate the concerted movement of loop 6. These differences compared to WT TIM are propagated in the ligand bound form in which V167 and T177 have different activation barriers for loop opening again suggesting that muta-

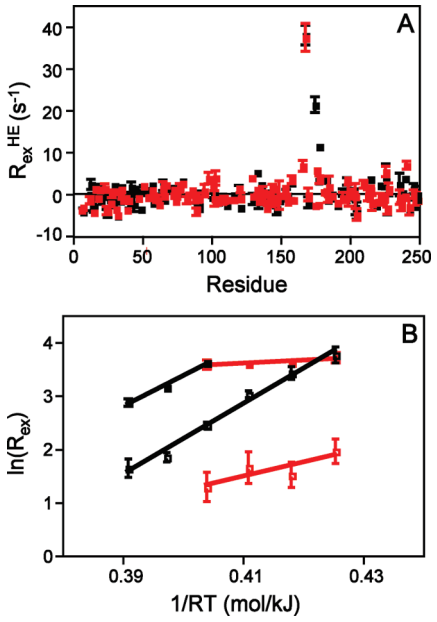

FIGURE 5: Chemical exchange contribution to R_2^β. (A) Residue-specific chemical exchange contribution to R_2^β of WT (black) and TGAG (red) cTIM at 298 K. (B) Temperature dependent relationship of R_{ex} for V167 (■) and T177 (□) in WT (black) and TGAG (red) cTIM. The activation energy for loop closure is extracted from the slope of the linear regression fit to the data points.

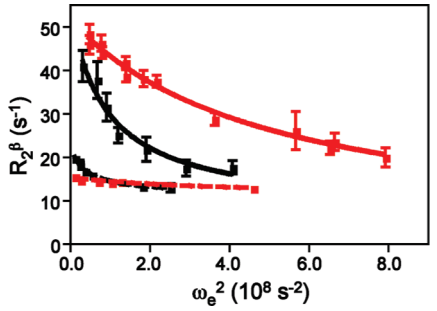

FIGURE 6: Conformational exchange in cTIM. TROSY-selected R_1^ρ dispersion curves for V167 (top) and T177 (bottom) in WT (black) and TGAG (red) cTIM measured at 298 K.

tion at loop 7 decouples the motion between the N- and C-terminal hinges of loop 6.

The different apparent activation barriers determined from the temperature dependence of R_{ex} for V167 and T177 in TGAG are contrasted with the identical k_{ex} values at 298 K. This suggests differing populations and/or different temperature dependencies of the open/closed populations for V167 relative to T177 in TGAG. As shown in eq 7, R_{ex} from the Hahn-Echo experiment depends not only on k_{ex} but on the populations as well.

On the basis of the coevolution of the N-terminal hinge of loop 6 and loop 7, it is expected that alteration of the loop 7 sequence would have significant functional consequences in the absence of the corresponding loop 6 sequence. While there are no direct interactions observed between the N-terminal hinge of loop 6 and loop 7, mutation of loop 7 to TGAG clearly has an effect on the N-terminal hinge of loop 6. In the TGAG mutant, the activation barrier for V167 is 5.9 ± 1.6 kJ/mol as compared to 57.6 ± 7.7 kJ/mol for WT TIM. Perhaps this reduction in the activation barrier for loop closure would be less pronounced if loop 7 (TGAG) encountered its correlated loop 6 N-terminal hinge (PPE). It is likely that the extra proline residue at the N-terminal hinge of loop 6 in archaeal TIM, which is usually found with TGAG, plays a role in enabling proper hydrogen bonding with the TGAG motif and thus allows the loop to move into the proper closed conformation.

Further understanding of the effects of the TGAG mutation can be gleaned from comparing the TGAG mutant described in this article with two other previously studied loop 7 mutants, Y208F and S211A (*3*, *8*, *10*). Both Tyr208 and Ser211 form hydrogen bonds with residues in loop 6 and thus play a crucial role in stabilizing the closed form of TIM. In the S211A mutant, a 30-fold reduction in catalytic efficiency was observed, likely due to the elimination of two hydrogen bonds (Figure 1). In the Y208F mutant, a 2500-fold reduction in catalytic efficiency was observed, indicating that the hydrogen bond between Tyr208 and Ala176 is crucial for TIM catalysis. The 240-fold reduction in catalytic efficiency observed for the TGAG mutant reflects an intermediate loss in efficiency compared to that of the S211A and Y208F mutant enzymes. On the basis of hydrogen bonding alone, it is expected that the efficiency of the TGAG mutant would be reduced relative to the S211A mutant but greater than the Y208F mutant. Assuming minimal perturbations to the active site, the distance between the side chain oxygen of Thr208 and Ala176 would be greater than the distance between Tyr208 and Ala176 in the wild-type enzyme, resulting in a weaker hydrogen-bonding interaction in the TGAG mutant. Thus, the diminished catalytic efficiency of the TGAG mutant is largely due to elimination of the hydrogen bonds formed by S211 and a weaker hydrogen bond between Thr208 and Ala176.

A quantitative investigation of the kinetics of loop motion is shown in Figure 6. Dispersion analysis for the TGAG mutant allowed for the determination of a k_{ex} value of 18,000 ± 2000 s^{-1} for both V167 and T177, in contrast to the k_{ex} value of 9000 ± 1500 s^{-1} for both residues in the WT enzyme. The fact that V167 and T177 could be fit together to determine k_{ex} suggests that the two hinges are participating in the same motional process. The elevated k_{ex} of TGAG loop 6 motion in the TGAG mutant compared to WT enzyme is consistent with the observation of lower activation barriers for loop closure in the TGAG mutant. However, the different activation barriers observed for the N- and C-terminal hinge residues in the TGAG mutant demonstrate that there is likely some loss in correlated motions contributing to the reduced catalytic efficiency of TGAG mutant TIM, perhaps due to different population distributions for V167 and T177. Elimination of hydrogen bonds by mutation of loop 7 clearly perturbs the motion of the active site loop. It seems that without proper assistance from loop 7, loop 6 undergoes conformational exchange between the open state and an imperfectly closed state at a higher rate.

The isotope exchange studies show that the fractional yield of *d*-GAP is not affected by the loop 7 mutation, indicating that after enolization of the substrate no additional water accesses the active site if regeneration of substrate (the back reaction) occurs. In contrast, the larger fraction of *d*-DHAP observed from the mutant catalyzed reaction indicates that the substrate-derived proton is more susceptible to solvent exchange in the reaction catalyzed by the TGAG mutant than in the reaction catalyzed by the WT enzyme once the enzyme commits to formation of the DHAP product. These biochemical data in combination with the faster loop 6 motion determined by NMR perhaps suggests that the faster, non-WT-like loop 6 motion occurs at the enediol

intermediate state of the reaction. These isotope exchange results further support the hypothesis of imperfect loop closure and indicate that as chemistry proceeds, loop 7 plays a crucial role in facilitating the coordinated motion of loop 6 with active site chemistry.

Biochemical studies and NMR investigations both support the notion that the interactions between loop 6 and loop 7 are essential to TIM function. By replacing 208-YGGS-211 in loop 7 with the corresponding naturally occurring sequence from an archaeal homologue, the sequence 166-PVW-168 in loop 6 loses its corresponding loop 7 partner. Detrimental effects in enzyme function are observed, with a marked loss in catalytic activity, binding specificity, and thermal stability. TROSY-Hahn-Echo and TROSY-selected $R_{1\rho}$ experiments suggest that apart from maintaining the proper chemical context, loop 7 also plays an important role in modulating chemical dynamics of loop 6 in order to ensure that both termini of loop 6 move in a concerted manner, as well as keeping a proper rhythm for chemistry to take place at the active site with maximum efficiency. Isotope exchange studies provide further investigation into the role of loop 7 along the reaction coordinate by suggesting that additional loop opening occurs in the midst of the chemical reaction in TGAG.

ACKNOWLEDGMENT

We acknowledge the helpful suggestions of John Richard and Tina Amyes at the 2008 Gordon Conference on Enzymes, Coenzymes and Metabolic Pathways. We thank Andy Mesecar and Scott Pegan for helpful comments and Professor Andrew Hamilton for the use of his CD spectrometer.

SUPPORTING INFORMATION AVAILABLE

Sequence alignment showing the occurrence of loop 6 and loop 7 sequences. This material is available free of charge via the Internet at http://pubs.acs.org.

REFERENCES

1. Hedstrom, L., Szilagyi, L., and Rutter, W. J. (1992) Converting trypsin to chymotrypsin: the role of surface loops. *Science 255*, 1249–1253.
2. Peng, T., Zintsmaster, J. S., Namanja, A. T., and Peng, J. W. (2007) Sequence-specific dynamics modulate recognition specificity in WW domains. *Nat. Struct. Mol. Biol. 14*, 325–331.
3. Venkitakrishnan, R. P., Zaborowski, E., McElheny, D., Benkovic, S. J., Dyson, H. J., and Wright, P. E. (2004) Conformational changes in the active site loops of dihydrofolate reductase during the catalytic cycle. *Biochemistry 43*, 16046–16055.
4. Wang, L., Pang, Y., Holder, T., Brender, J. R., Kurochkin, A. V., and Zuiderweg, E. R. (2001) Functional dynamics in the active site of the ribonuclease binase. *Proc. Natl. Acad. Sci. U.S.A. 98*, 7684–7689.
5. Watt, E. D., Shimada, H., Kovrigin, E. L., and Loria, J. P. (2007) The mechanism of rate-limiting motions in enzyme function. *Proc. Natl. Acad. Sci. U.S.A. 104*, 11981–11986.
6. Akke, M., Liu, J., Cavanagh, J., Erickson, H. P., and Palmer, A. G. (1998) Pervasive conformational fluctuations on microsecond time scales in a fibronectin type III domain. *Nat. Struct. Biol. 5*, 55–59.
7. Siggers, K., Soto, C., and Palmer, A. G.3rd (2007) Conformational dynamics in loop swap mutants of homologous fibronectin type III domains. *Biophys. J. 93*, 2447–2456.
8. Rozovsky, S., and McDermott, A. E. (2007) Substrate product equilibrium on a reversible enzyme, triosephosphate isomerase. *Proc. Natl. Acad. Sci. U.S.A. 104*, 2080–2085.
9. Joseph, D., Petsko, G. A., and Karplus, M. (1990) Anatomy of a conformational change: Hinged "lid" motion of the triosephosphate isomerase loop. *Science 249*, 1425–1428.
10. Williams, J. C., and McDermott, A. E. (1995) Dynamics of the flexible loop of triosephosphate isomerase: the loop motion is not ligand gated. *Biochemistry 34*, 8309–8319.
11. Berlow, R. B., Igumenova, T. I., and Loria, J. P. (2007) Value of a hydrogen bond in triosephosphate isomerase loop motion. *Biochemistry 46*, 6001–6010.
12. Desamero, R., Rozovsky, S., Zhadin, N., McDermott, A., and Callender, R. (2003) Active site loop motion in triosephosphate isomerase: T-Jump relaxation spectroscopy of thermal activation. *Biochemistry 42*, 2941–2951.
13. Massi, F., Wang, C., and Palmer, A. G.3rd (2006) Solution NMR and computer simulation studies of active site loop motion in triosephosphate isomerase. *Biochemistry 45*, 10787–10794.
14. Rozovsky, S., Jogl, G., Tong, L., and McDermott, A. E. (2001) Solution-state NMR investigations of triosephosphate isomerase active site loop motion: ligand release in relation to active site loop dynamics. *J. Mol. Biol. 310*, 271–280.
15. Rozovsky, S., and McDermott, A. E. (2001) The time scale of the catalytic loop motion in triosephosphate isomerase. *J. Mol. Biol. 310*, 259–270.
16. Sampson, N. S., and Knowles, J. R. (1992) Segmental motion in catalysis: investigation of a hydrogen bond critical for loop closure in the reaction of triosephosphate isomerase. *Biochemistry 31*, 8488–8494.
17. Pompliano, D. L., Peyman, A., and Knowles, J. R. (1990) Stabilization of a reaction intermediate as a catalytic device: Definition of the functional role of the flexible loop in triosephosphate isomerase. *Biochemistry 29*, 3186–3194.
18. Sampson, N. S., and Knowles, J. R. (1992) Segmental movement: Definition of the structural requirements for loop closure in catalysis by triosephosphate isomerase. *Biochemistry 21*, 8482–8487.
19. Kempf, J. G., Ju-yeon, J., Ragain, C., Sampson, N. S., and Loria, J. P. (2007) Dynamic requirements for a functional protein hinge. *J. Mol. Biol. 368*, 141–149.
20. Sun, J., and Sampson, N. S. (1998) Determination of the amino acid requirements for a protein hinge in triosephosphate isomerase. *Protein Sci. 7*, 1495–1505.
21. Sun, J., and Sampson, N. S. (1999) Understanding protein lids: Kinetic analysis of active hinge mutants in triosephosphate isomerase. *Biochemistry 38*, 11474–11481.
22. Xiang, J., Sun, J., and Sampson, N. S. (2001) The importance of hinge sequences for loop function and catalytic activity in the reaction catalyzed by triosephosphate isomerase. *J. Mol. Biol. 307*, 1103–1112.
23. Xiang, J. Y., Jung, J. Y., and Sampson, N. S. (2004) Entropy effects on protein hinges: The reaction catalyzed by triosephosphate isomerase. *Biochemistry 43*, 11436–11445.
24. Kursula, I., Salin, M., Sun, J., Norledge, B. V., Haapalainen, A. M., Sampson, N. S., and Wierenga, R. K. (2004) Understanding protein lids: structural analysis of active hinge mutants in triosephosphate isomerase. *Protein Eng. Des. Sel. 17*, 375–382.
25. Lolis, E., Alber, T., Davenport, R. C., Rose, D., Hartman, F. C., and Petsko, G. A. (1990) Structure of yeast triosephosphate isomerase at 1.9-Å resolution. *Biochemistry 29*, 6609–6618.
26. Lolis, E., and Petsko, G. A. (1990) Crystallographic analysis of the complex between triosephosphate isomerase and 2-phosphoglycolate at 2.5-Å resolution: implications for catalysis. *Biochemistry 29*, 6619–6625.
27. Zhang, Z., Sugio, S., Komives, E. A., Liu, K. D., Knowles, J. R., Petsko, G. A., and Ringe, D. (1994) Crystal structure of recombinant chicken triosephosphate isomerase-phosphoglycolohydroxamate complex at 1.8-Angstrom resolution. *Biochemistry 33*, 2830–2837.
28. Plaut, B., and Knowles, J. R. (1972) pH-dependence of the triose phosphate isomerase reaction. *Biochem. J. 129*, 311–320.
29. O'Donoghue, A. C., Amyes, T. L., and Richard, J. P. (2005) Hydron transfer catalyzed by triosephosphate isomerase. Products of isomerization of (R)-glyceraldehyde 3-phosphate in D2O. *Biochemistry 44*, 2610–2621.
30. Loria, J. P., Rance, M., and Palmer, A. G. (1999) Transverse-relaxation-optimized (TROSY) gradient-enhnaced triple-resonance NMR spectroscopy. *J. Magn. Reson. 141*, 180–184.
31. Pervushin, K., Riek, R., Wider, G., and Wuthrich, K. (1997) Attenuated T2 relaxation by mutual cancellation of dipole-dipole coupling and chemical shift anisotropy indicates an avenue to NMR structures of very large biological macromolecules in solution. *Proc. Natl. Acad. Sci. U.S.A. 94*, 12366–12371.
32. Wittekind, M., and Mueller, L. (1993) HNCACB, a high-sensitivity 3D NMR experiment to correlate amide-proton and nitrogen resonances with the alpha- and beta-carbon resonances in proteins. *J. Magn. Reson., Ser. B 101*, 201–205.
33. Delaglio, F., Grzesiak, S., Vuister, G., Zhu, G., Pfeifer, J., and Bax, A. (1995) NMRPipe: a multidimensional spectral processing system based on UNIX pipes. *J. Biomol. NMR 6*, 277–293.
34. Goddard, T., and Kneller, D. G. *SPARKY 3*, University of California, San Francisco, CA.

35. Cole, R., and Loria, J. P. (2002) Evidence for flexibility in the function of ribonuclease A. *Biochemistry 41*, 6072–6081.
36. Press, W. H., Flannery, B. P., Teukolsky, S. A., and Vetterling, W. T. (1986) *Numerical Recipes. The Art of Scientific Computing*, 2nd. ed., Cambridge University Press, Cambridge, UK.
37. Igumenova, T. I., and Palmer, A. G.III (2006) Off-resonance TROSY-selected R 1rho experiment with improved sensitivity for medium- and high-molecular-weight proteins. *J. Am. Chem. Soc. 128*, 8110–8111.
38. Palmer, A. G., Kroenke, C. D., and Loria, J. P. (2001) Nuclear magnetic resonance methods for quantifying microsecond-to-millisecond motions in biological macromolecules. *Methods Enzymol. 339* (Part B), 204–238.
39. Kempf, J. G., and Loria, J. P. (2004) Measurement of Intermediate Exchange Phenomena, in *Protein NMR Techniques* (Downing, A. K., Ed.) pp 185−231, Humana Press, Totowa, NJ..
40. Ugurbil, K., Garwood, M., and Rath, A. R. (1988) Optimization of modulation functions to improve insensitivity of adiabatic pulses to variations in B_1 magnitude. *J. Magn. Reson. 80*, 448–469.
41. Garwood, M., and Ke, Y. (1991) Symmetric pulses to induce arbitrary flip angles with compensation of RF inhomogeneity and resonance offsets. *J. Magn. Reson. 94*, 511–525.
42. Mulder, F. A. A., de Graaf, R. A., Kaptein, R., and Boelens, R. (1998) An off-resonance rotating frame relaxation experiment for the investigation of macromolecular dynamics using adiabatic rotations *J. Magn. Reson. 131*, 351–357.
43. Wang, C., Rance, M., and Palmer, A. G. (2003) Mapping chemical exchange in proteins with MW > 50 kD. *J. Am. Chem. Soc. 125*, 8968–8969.
44. Butterwick, J. A., Loria, J. P., Astrof, N. S., Kroenke, C. D., Cole, R., Rance, M., and Palmer, A. G.3rd (2004) Multiple time scale backbone dynamics of homologous thermophilic and mesophilic ribonuclease HI enzymes. *J. Mol. Biol. 339*, 855–871.
45. Evenas, J., Forsen, S., Malmendal, A., and Akke, M. (1999) Backbone dynamics and energetics of a calmodulin domain mutant exchanging between closed and open conformations. *J. Mol. Biol. 289*, 603–617.
46. Mandel, A. M., Akke, M., and Palmer, A. G. (1996) Dynamics of ribonuclease H: temperature dependence of motions on multiple time scales. *Biochemistry 35*, 16009–16023.
47. O'Donoghue, A. C., Amyes, T. L., and Richard, J. P. (2005) Hydron transfer catalyzed by triosephosphate isomerase. Products of isomerization of dihydroxyacetone phosphate in D2O. *Biochemistry 44*, 2622–2631.